Characterizing Single Electron Radiation in an Intense Laser Field

Caleb Coburn

A senior thesis submitted to the faculty of
Brigham Young University
in partial fulfillment of the requirements for the degree of

Bachelor of Science

Michael Ware, Advisor

Department of Physics and Astronomy

Brigham Young University

August 2013

ABSTRACT

Characterizing Single Electron Radiation in an Intense Laser Field

Caleb Coburn
Department of Physics and Astronomy
Bachelor of Science

We report the intensity measurement of a high intensity pulsed laser focus and the efficiency characterization of an optical signal collection system. We seek experimental confirmation that large free electron wave packets radiate like point particles. Our experiment requires intensities on the order of 10^{18} W/cm^2 to produce red-shifted signal photons. The red shift is important in discriminating against a large background. We use time-of-flight spectroscopy to measure the charge to mass ratio of laser induced multiply ionized argon and compare the highest achieved charge state with known strong-field ionization i ntensities. We also use parametric down conversion to make an absolute efficiency measurement of our detection system. These measurements are necessary to ensure our apparatus is capable of producing the intensity dependent signal that we seek and allow us to calculate the total radiated signal. We measure a pulse intensity of at least 1.57×10^{18} W/cm^2. The collection efficiency is $22.7 \pm 1\%$. This work was supported by the National Science Foundation (Grant No. PHY-0970065).

Keywords: [single electron radiation, large wave packet, high-intensity laser, photoemission, scattering, quantum optics]

ACKNOWLEDGMENTS

I would like to acknowledge the financial support of the National Science Foundation as well as the BYU Physics department. I would also like to thank Dr. Ware and Dr. Peatross for their leadership, guidance, and help in completing the work for this thesis. Finally, I appreciate the support of my wife Jessica.

Contents

List of Figures

List of Tables

Chapter 1

Introduction

1.1 Single Electron Photoemission

What exactly is an electron? While we know much about the nature of electrons, our understanding is still limited. For example, we do not know if electrons are truly elementary particles and there is a search for a non-zero dipole moment. The work reported in this thesis is part of a larger experiment that seeks to clarify the quantum mechanical description of electrons.

Quantum mechanics introduces the concept of wave-particle duality, which holds that all matter exhibits both wave and particle properties. All particles exhibit this dual nature; however, with macroscopic objects the effect is negligible. On the other hand, as we examine particles on a microscopic scale, their wave nature becomes important.

Single electrons exhibit wave properties. This can be seen in single electron double-slit experiments. In this type of experiment electrons pass through a double-slit and the position of their impact on a screen behind the slits is recorded. The result of recording many electrons' position on the screen is a double slit interference pattern, just like that of Young's double-slit experiment done with coherent light. The interference is observed even though the electrons pass through the

slits one at a time [1]. This implies that the electron is interfering with itself, which is not possible for a classical particle.

The wave nature of the electron can be described by its wave function, which contains all information about the electron. The wave function multiplied with its complex conjugate gives the probability distribution of finding the electron in a region of space. Also, due to the Heisenberg uncertainty relation $\Delta x \Delta p \geq \hbar/2$, any finite certainty in the momentum Δp must be accompanied by a finite uncertainty in position Δx. An electron's wave packet is then necessarily spread out in space. It is not intuitive that the particle's position can only be determined to be within some region and not absolutely. As a result it is tempting to think of an electron's properties, such as mass and charge, as being spread out over the probability distribution.

While an electron occupies a bound state of an atomic potential, its wave packet remains localized around the atom. In contrast, the wave packet of a free electron expands rapidly. If the initial position of the electron is confined to about the size of an atom, its wave packet can expand to the scale of optical wavelengths within about 100 fs [2]. Interaction with a laser field can cause the wave packet to spread further as it experiences different phases of the laser field [3].

An opportunity to help clarify the correct interpretation of an electron's charge distribution arises from examining the radiation scattered from these large electron wave packets. There is a measurable difference for how an electron radiates between the point emitter and extended charge distribution models [4]. Radiation from an extended charge distribution is suppressed due to destructive interference between different regions of the charge distribution. This interference occurs when different regions of the large wave packet experience different phases of the laser cycle and accelerate in opposite directions. The predicted radiated intensity differs by about two orders of magnitude from a point emitter [5]. By measuring the radiation scattered by free electrons in an intense laser focus and comparing with calculated expected values for both models we can investigate experimentally whether large electron wave packets radiate like point emitters or extended

charge distributions.

1.2 Relevant Work in Literature

Single electron dynamics in intense laser fields have received significant attention since high-intensity pulse lasers have become more widely available [3, 4, 6–8]. These studies address topics such as how single electron wave packets evolve in time in intense laser fields, how they scatter the intense laser light, how relativistic and kinematic effects influence scattered light, and other characteristics of single electron radiation.

A correct model for how single electrons scatter laser light is important for calculating expected scattered radiation from intense laser foci. There are a couple examples in literature where the extended charge distribution has been used to calculate scattered light [3, 6]. We feel that this is incorrect based on the predictions of quantum electrodynamics (QED), as discussed in the section 1.3. In both of these papers the scattered light is calculated by using the product of the probability current by the electron charge as a source term in Maxwell's equations. This causes destructive interference to suppress radiation emitted at 90° from the direction of the driving laser field. One result of this formulation is that infinitely large wave packets do not radiate. We seek experimental confirmation that large electron wave packets will radiate as strongly as point particles.

1.3 Previous Work on the Overall Experiment

Work on the overall experiment is ongoing. Previous to the work reported in this thesis, our quantum optics research group, headed by Dr. Ware and Dr. Peatross, constructed the experimental apparatus and did theoretical modeling for point and extended charge distribution models.

John Corson *et al.* modeled a single-electron wave packet in an intense laser field [5, 9]. The authors used quantum electrodynamics to account for the quantization of the light field as well as

of the electron. Their findings predict that an electron wave packet will radiate as a point particle and not as an extended charge distribution.

In their paper [9], Corson *et al*. outline a QED model of single electron photon scattering. Their method is to apply the Born probability interpretation to the projections of the second-quantized entangled electron-photon state onto pure plane-wave states. A single electron's radiation can be represented as a superposition of plane-wave states. To calculate the probability of an observable measurement one projects the normalized state onto an eigenstate of the measurement. The probability is then the sum of the projection amplitude squared. Thus, when calculating scattering probabilities, one squares the magnitude of the contributions from the projection of the state onto plane-wave components and then sums them. This causes complex phases to drop out of the calculation before they are allowed to interfere. Said another way, $|\Psi_1|^2 + |\Psi_2|^2 \neq |\Psi_1 + \Psi_2|^2$. The plane-wave components are incoherent so $|\Psi_1|^2 + |\Psi_2|^2$ is the correct approach. Spreading of a wave packet over time is determined by a time dependent complex phase. As a result, the probability of scattering is independent of the spatial extent of the wave packet. This supports the point emitter model of single electron radiation.

To experimentally support this prediction we need to know the predicted radiative strength of an electron in an intense laser focus according to both models. For an extended charge distribution, radiation is suppressed relative to that of a point emitter in all directions but along the axis of the laser propagation as the wave packet reaches the size of the wavelength of the driving field [10]. Peatross *et al.* modeled radiation from an extended charge distribution driven by a plane wave. They found that the radiated power out the side of the laser focus (perpendicular to the axis of laser propagation and polarization) is suppressed by two orders of magnitude compared with a point-like emitter [4]. We can observe radiation in the perpendicular direction and compare with computational predictions for both models. The large disparity between the radiating strengths of each model should allow us to conclude which correctly predicts single electron radiation.

1.4 Overview of Thesis

We combine ultra-high intensity lasers and quantum optics to stimulate and detect single electron radiation. This is an unusual combination that brings with it some difficulties, such as detecting single photons emitted from a free electron over the background noise of the ionizing laser beam. Discriminating against the huge background of laser light to detect scattered light is essential to making an accurate measurement.

We approach this in multiple ways, including spectral and temporal filtering of our signal. We are able to filter spectrally because the free electrons are accelerated in to mildly relativistic speeds ($\approx 3*10^7$ m/s or $\beta \approx .1$) in the laser focus and some emitted photons will be observed to be significantly Doppler shifted. Electrons in an intense laser focus are accelerated forward in an effect called the Lorentz drift. The Lorentz drift is a net forward acceleration due to the electron's interaction with the oscillating electric and magnetic field of the laser via $\vec{F} = q(\vec{E} + \vec{v} \times \vec{B})$. If the driving laser field reaches sufficiently high intensities ($\approx 10^{18}$ W/cm^2), ponderomotive gradients accelerate electrons to relativistic speeds. As a result, some of the emitted photons, observed laterally from the focus, will be red-shifted from the wavelength of the laser pulse. We can take advantage of this red-shift to detect the signal over the background.

To find predicted values for single electron radiation strengths, we model radiation from a point-like electron by first calculating possible electron trajectories numerically. We then use the trajectory to calculate expected radiated power. As shown in Fig. 1.1(a), the point charge is a strong emitter in all but the $\hat{x}$ direction. The red-shifted signal is only emitted in the perpendicular directions. Fortuitously, the direction in which single electrons emit red-shifted signal photons is the same direction for which radiation from an extended charge distribution would be suppressed. This allows us to observe the signal from the laser focus over the background noise in a direction for which point and extended charge distributions radiate differently. From our numerical calculations we expect about one red-shifted photon per 300 laser pulses if the electron radiates as a point

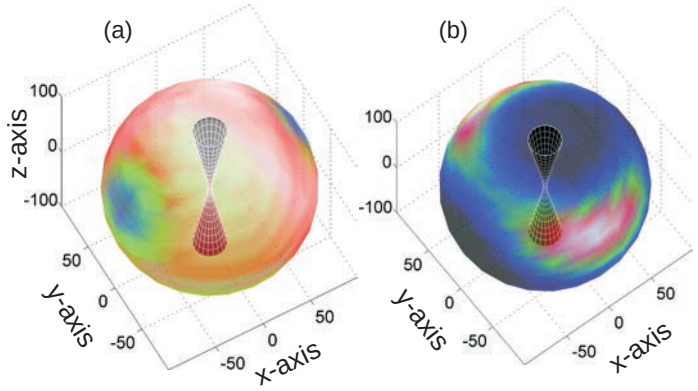

Figure 1.1 Point charge radiated intensity, showing the intensity of scattered radiation as function of angle. The emitters are driven by an intense laser field. On the left (a) is the pattern for a point electron. On the right (b) is red-shifted emission for the same point electron. Radiated intensity of red-shifted photons occurs perpendicular to the laser focus.

particle, and about one in 1000 if the electron radiates as an extended charge distribution [10].

In this thesis we report work contributing to two essential aspects of an overall experiment designed to observe single electron radiation: laser focus intensity measurements and the signal collection system efficiency calibration. Our experiment requires intensities sufficient to cause radiation scattered by electrons perpendicular to the laser axis and polarization to be red shifted. In order to produce definitive results we must ensure we obtain intensities of at least 10^{18} W/cm^2 [10]. We also need to understand our collection system efficiency in order to calculate total radiated power.

In Chapter 2 I explain the apparatus and major components of key systems. I also discuss methods for measuring intensity at the laser focus, and characterizing the collection system efficiency.

In Chapter 3 I discuss the results of intensity and collection efficiency measurements. I also analyze these results and discuss the direction of further work on the experiment.

Chapter 2

Experimental Methods

This chapter explains the apparatus used to measure single electron radiation and details the methods for the specific measurements reported in this thesis. In sections 2.1 to 2.6 we describe important components of the apparatus to help the reader understand the context of the reported measurements. In sections 2.7 and 2.8 we explain the calibration of the collection system and the intensity measurement, respectively.

2.1 Overview of the Electron Radiation Experiment

The overall goal of our experiment is to observe light scattered by free electrons perpendicular to the axis of propagation of an intense laser focus. We expect to measure a radiated power that corresponds to theory for either point-like or extended charge distribution photo emission, as described in Chapter 1.

Our experimental apparatus creates free electrons and observes the radiation they emit when they oscillate in the laser field. We use an intense laser pulse to ionize helium atoms. The electrons pulled away from the helium atoms in the laser focus become the free electrons that we observe. We then use an optical collection system to look for light scattered by the free electrons to determine

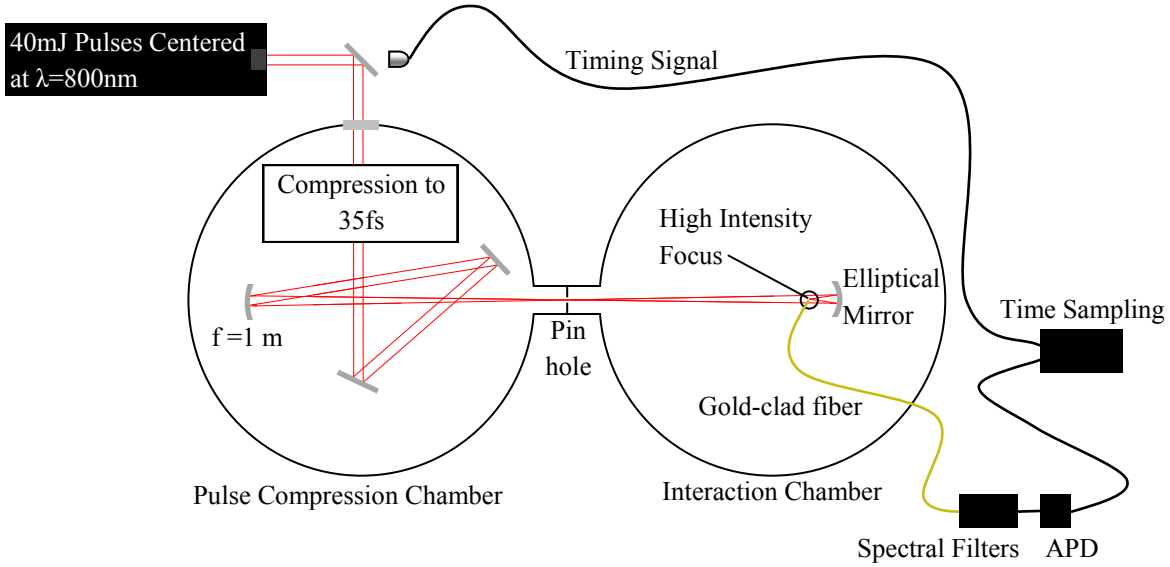

Figure 2.1 An overview of the experimental setup, showing a simplified beam path. Laser pulses enter the vacuum chambers, compressed, and focused. Free electrons in the focus radiate signal photons. A gold clad fiber collects these signal photons via a one-to-one imager above the focus.

how strongly they radiate. Detecting the signal is difficult, however, because the ionizing laser contains about 19 orders of magnitude more photons than our signal. This light can scatter off the apparatus and enter our optical collection system. We overcome this obstacle by using the characteristic red shift and timing relative to the driving pulse of the signal photons to discriminate against the large background, as discussed in sec. 1.4.

The red shift is created when the laser field is strong enough to accelerate electrons relativistically. This raises the required intensity from about 8.7×10^{15} W/cm^2 (the intensity needed to fully ionize He [11]) to around 10^{18} W/cm^2.

The layout of the experiment is given in Fig. 2.1. Pulses from the laser system are brought into the pulse compression chamber where they are compressed temporally by a series of reflections off diffraction gratings. The compressed pulse is then reflected off of a 1m focal length spherical lens. This focuses the beam through a pinhole separating the two chambers. Inside the interaction

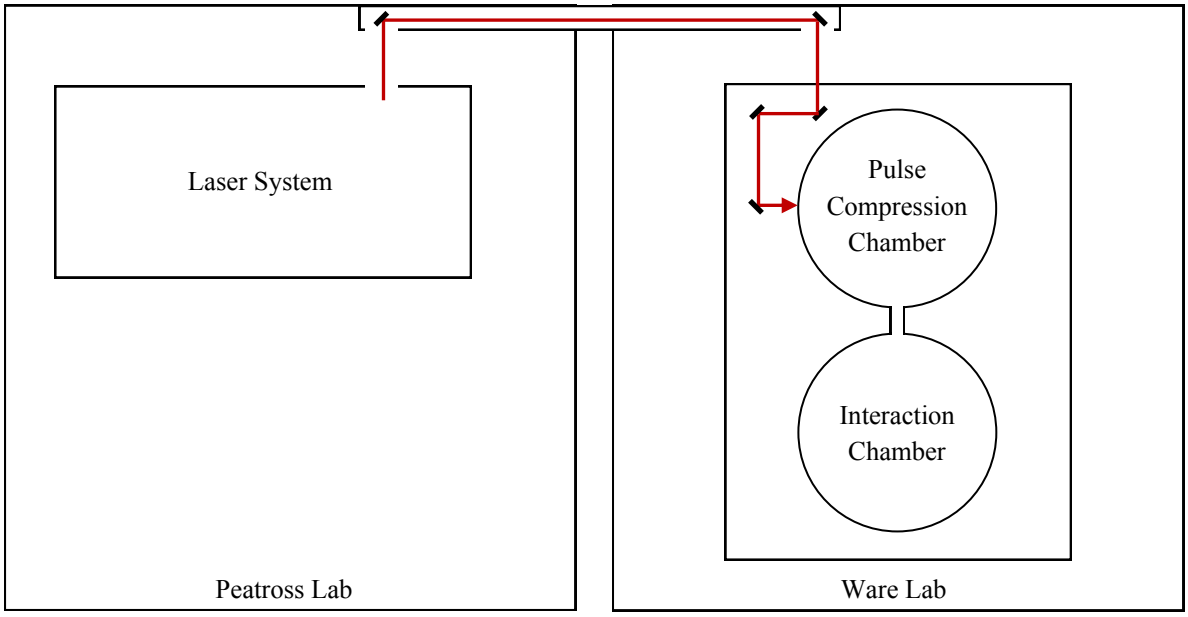

Figure 2.2 The layout of the laser and vacuums system between the Peatross and Ware labs. Chirped pulses from the laser system in the Peatross lab are directed through a pipe into the Ware lab and finally into the pulse compression chamber.

chamber the pulse is focused tightly by an elliptical mirror. The most intense regions of the focus will reach intensities high enough stimulate free electrons to emit photons that are red-shifted from $\lambda = 800$ nm to $\lambda = 890$ nm. Some of these are collected by a one-to-one imager directly above the laser focus. This couples the photons into a fiber optic cable which carries the signal out of the interaction chamber. It is sent through spectral filters before arriving at a single photon detector. We also collect a timing signal from the pulse before it enters the chamber that allows us to discriminate against noise that arrives at the detector at the wrong time.

Our experiment has components in two laboratories, the Peatross lab and the Ware lab. The layout of the experiment in the labs in given in Fig. 2.2. The laser system is in the Peatross lab. The two labs are connected by a pipe with an opening at both ends. We direct the laser from the Peatross lab through the pipe into the Ware lab.

2.2 Laser System

Our laser system is located in the Peatross lab. It is an 800 nm titanium:sapphire pulse laser capable of 40–100 mJ per pulse with a pulse duration of about 35 fs. The pulse repetition rate is 10 Hz.

The laser system generates our pulses via chirped pulse amplification (CPA). CPA takes a pulse with a long spectral bandwidth, stretches it out in time, and amplifies it in its stretched form. This is beneficial because chirping the pulse, or stretching it out temporally, decreases the pulse intensity enough to avoid damaging the gain medium, a titanium:sapphire crystal, and the other optics.

Chirping is introduced into the pulse as it propagates through air and lenses. As it travels through these media the pulse spreads out temporally, becoming a longer pulse. This happens because the index of refraction is dependent on wavelength: A high frequency photon experiences a slightly higher index of refraction than lower frequencies. This delays the higher frequency components relative to the lower frequency components and creates a chirped pulse.

The pulses are amplified to the final pulse power before exiting the laser system in the Peatross lab. We adjust the power used to energize the gain medium to control pulse power. Even though the pulse does not gain any more energy after this point, it is still not at peak intensity. To realize the high intensities it must be temporally compressed (have its chirping removed) before the interaction. The chirping is removed in the pulse compression chamber.

2.3 Pulse Compression Chamber

The pulse compression chamber uses diffraction gratings to correct for the chirping from the laser pulses, as described in Fig. 2.3. Diffraction gratings separate the pulse's frequency components. They are aligned such that delayed wavelengths follow shorter paths before recombining, as shown in Fig. 2.3. The difference in path length can be adjusted in the alignment of the gratings, allowing us to add or remove chirping as desired. Also, it is necessary to perform the compression under

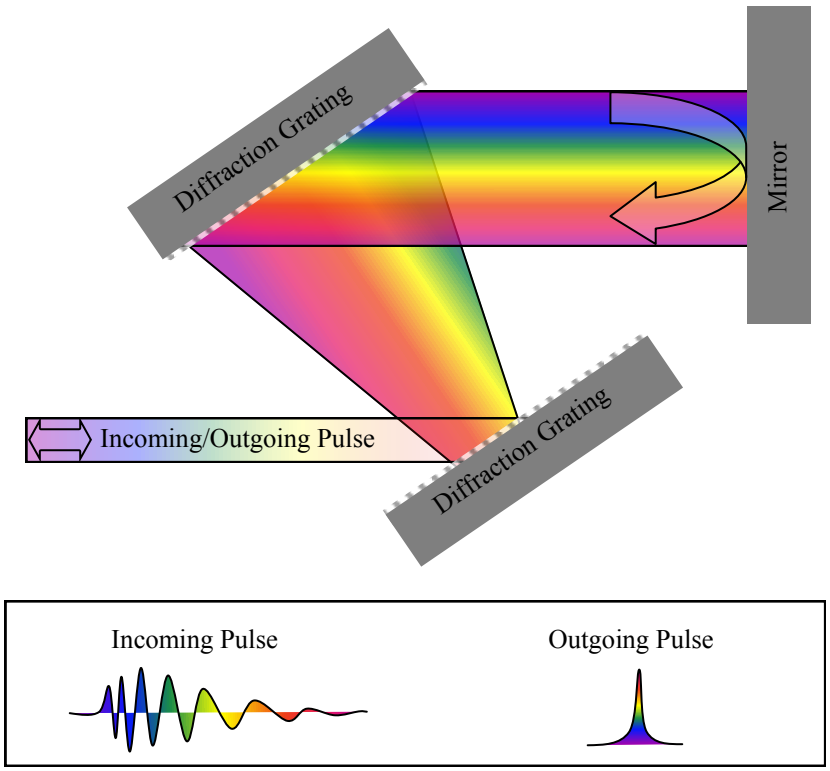

Figure 2.3 Chirped pulse compression: A basic setup for temporally compressing an incoming chirped pulse. Due to the alignment of the gratings, the pulse is spread out in space and the round trip path length is different for constituent wavelengths. This allows us to remove the chirping.

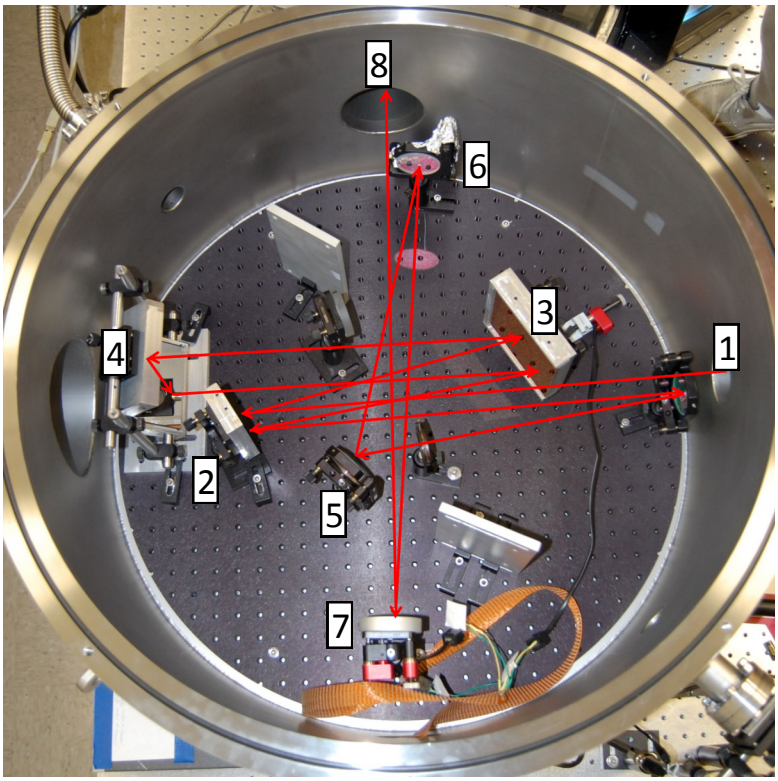

Figure 2.4 The beam path inside the pulse compression chamber. The pulse enters from a port at (1), reflects off of diffraction gratings (2) and (3), is shifted down down by periscope mirror (4), reflects off both gratings again, and then reflects off the flat mirror below port (1), reflects off flat mirrors (5) and (6), and finally is focused by spherical mirror (7) through a pinhole in port (8), which leads to the interaction chamber.

vacuum to avoid interaction between air and the pulse after temporal compression. The pulse compression chamber is maintained around 10^{-6} torr.

The beam is diverging slowly as it arrives at the window after traveling several meters from the laser system in the Peatross lab. Removing the chirping with the diffraction gratings, however, requires the beam be collimated. To fix this we use an appropriate converging lens as the window into the compression chamber to collimate the beam.

The beam path inside the pulse compression chamber is shown in Fig. 2.4. The collimated beam is directed into a set of diffraction gratings (analogous to Fig. 2.3) that remove the chirp. It is then directed onto a one meter focal length mirror, which focuses the pulse through a pinhole

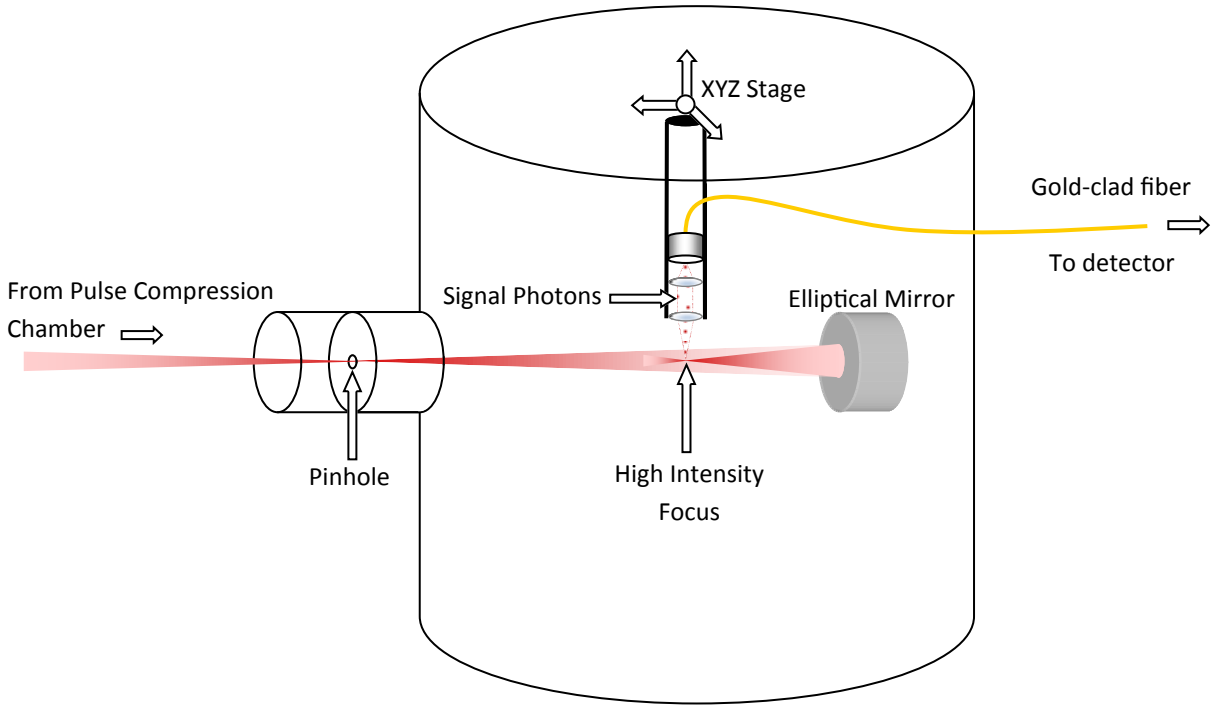

Figure 2.5 Interaction Chamber: the pulse enters from the pulse compression chamber and is focused by an elliptical mirror. Relativistic electrons in the focus emit red-shifted photons out the side of the focus, which are collected by the one-to-one imager above. The photons are then directed out of the chamber to the detector. Not shown are the vacuum pumps and a leak valve through which the chamber is backfilled with He.

separating the pulse compression chamber and the interaction chamber. Because of the larger beam waist, the focus at the pinhole does not reach the high intensities needed to produce red-shifted photons. The pulse enters the interaction chamber as it passes through the pinhole.

2.4 Interaction Chamber

The interaction chamber allows us to control the environment in which we ionize He (or other gasses for making intensity measurements) and observe the signal. The interaction chamber is initially pumped down to under 5×10^{-8} torr, a much higher vacuum than the pulse compression chamber. This allows us to obtain a purity of 1000 ppm when we backfill the chamber with He to

pressures around 10^{-6} torr.

The layout of the interaction chamber is given in Fig. 2.5. The laser pulse enters through the pinhole and is tightly focused by an elliptical mirror. This is the focus that reaches intensities high enough to create a red shift in photons scattered off free electrons. The collection system is positioned vertically over the focus on a stage with three degrees of freedom.

Temporal filtering plays an important role in detecting the signal above the noise. We use a large chamber (76 cm tall, 71 cm in diameter) so that there is a significant path difference and corresponding delay for stray light that takes an indirect path to the optical collection system. We measure the delay between detecting the pulse upstream and the signal arriving at the detector. We use this information and fast timing electronics with better than nanosecond resolution to pick out the real data from the detector response.

2.5 Vacuum and Gas Backfill Systems

The vacuum system consists of both chambers, the compression and interaction chambers, two turbo-fan pumps and a dry-scroll roughing pump. A vertical view of the vacuum system is given in Fig. 2.6. The roughing pump roughs both chambers as well as backing the turbo pump on the pulse compression chamber. This turbo pump then backs the turbo pump on the interaction chamber. Diffusion between the two chambers in restricted by the pinhole. This differential pumping allows the interaction chamber to reach vacuum pressures around 10^{-8} torr. Gasses can be introduced into the interaction chamber through a leak valve. The connection between the chambers is re-enforced to avoid movement due to the pressure difference across the pinhole. We can control the rate of gas flow into the interaction chamber to control the equilibrium pressure inside the chamber while taking data. We use this to control the average number of atoms in the focus.

The vacuum chambers have a large volume and surface area. To expedite pump-down time

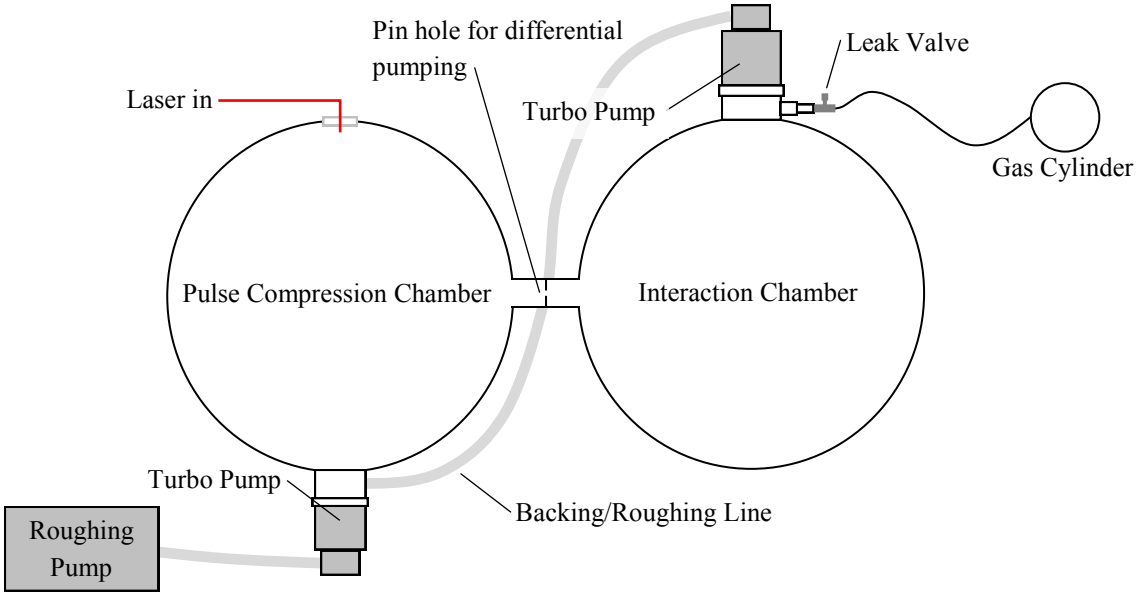

Figure 2.6 The vacuum system. The roughing pump backs the turbo pump connected to the compression chamber, which in turn backs the turbo pump connected to the interaction chamber. The leak valve for backfilling with a target gas is connected to the same flange as the turbo pump on the interaction chamber. Differential pumping across the pinhole creates a higher vacuum in the interaction chamber by about a factor of 100.

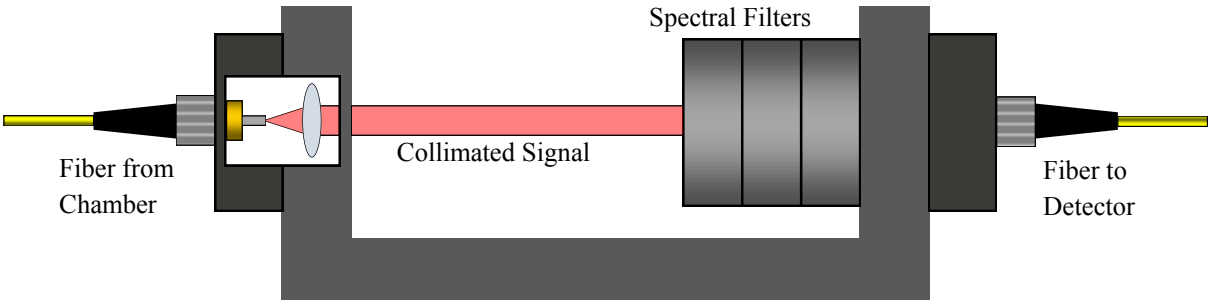

Figure 2.7 The signal exiting the interaction chamber in the gold clad fiber is collimated before passing through the spectral filters. After the filters it is focused back into a second length of fiber optic cable leading to the detector.

to vacuum levels needed in our experiment we wrap the interaction chamber with heating coils capable of reaching 200°C.

2.6 Optical Collection System

The optical collection system collects light emitted from the focus and directs it into the single photon detector. It consists of a one-to-one imager that channels light from the high intensity focus into a fiber optic cable. The cable is gold clad to prevent light from entering through the cladding and contaminate the signal. The fiber launch and imager are mounted on a cage system that is connected to a three way stage. This allows us to align the one-to-one imager with the laser focus. The fiber exits the chamber and carries the signal to a free space fiber coupler, shown in Fig. 2.7. The signal photons are collimated, pass through a high-pass and a band-pass filter, and then are coupled back into another fiber optic cable. By using the filters to screen the signal, noise that reaches the detectors is significantly reduced [10]. The outgoing cable guides the signal into a single photon detector.

Combining temporal and spectral filtering allows us to detect the signal even though it is 19 orders of magnitude smaller than the background.

2.7 Collection System Efficiency Callibration

The optical collection system efficiency is the ratio of signal emitted in the solid angle captured by the one-to-one imager to the signal detected. We used two methods to calibrate the efficiency of our optical collection system. The first method is a relative calibration that relies on the accuracy of the power meter we used to make the measurement. The second method is an absolute calibration, meaning that is is independent of all instrument calibrations. The absolute calibration is the primary measurement. The relative measurement provides a check on the absolute measurement. Also, the signal strength of the relative method using a diode laser is much greater than the absolute signal strength using down-converted photons. This makes aligning the system quicker and easier than the absolute method. After doing the relative measurement, we can switch switch the input signal between methods without significantly misaligning the collection system. This gives us a starting alignment for the absolute method and expedites the absolute alignment process.

2.7.1 Relative Calibration

The relative measurement is made using a 890 nm diode laser and an optical power meter. We use 890 nm light because this is the same wavelength as the red-shifted signal. The setup for this measurement is shown in Fig. 2.8. We couple the laser into a single mode fiber, which simulates the laser focus as in the absolute measurement. Next we align each component in the optical collection system individually to maximize efficiency. These components include: the angle of the fiber simulating the laser focus, the spatial position of the one-to-one imager, and the coupling between fibers at the spectral filtering apparatus. We then measure the power at points (b) and (c) in the figure with the power meter. The ratio of the power at (c) to the power at (a) is the optical collection system efficiency. The ratio of the power at (b) to the power at (a) tells us what the part of the power is collected by the one-to-one imager.

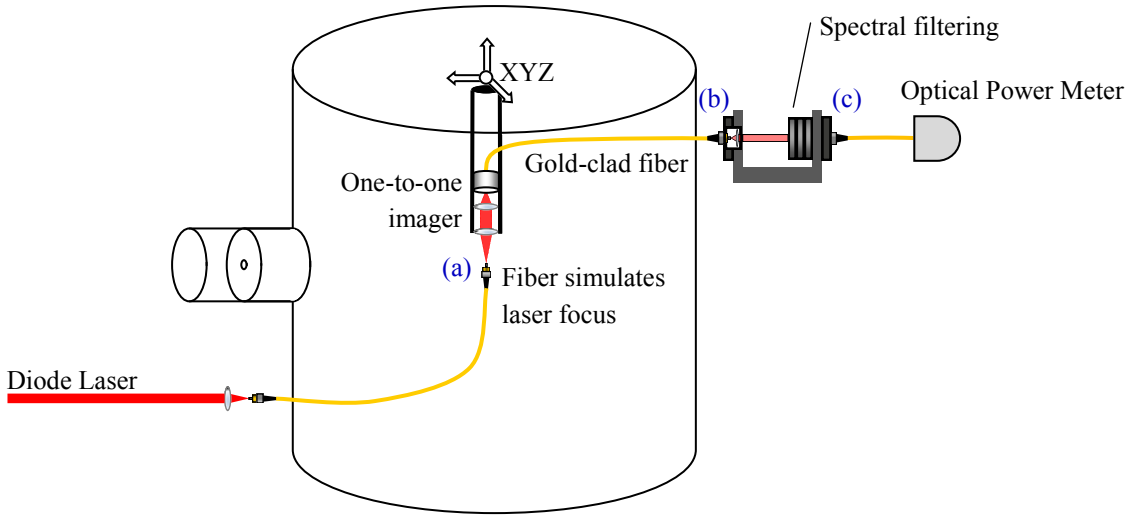

Figure 2.8 The relative efficiency measurement setup. Light from a diode laser is coupled into a fiber optic cable, which terminates in the interaction chamber at point (a) and simulates a laser focus. The power is measured at point (b) directly before the spectral filtering and at point (c) after the spectral filtering.

2.7.2 Absolute Calibration

The absolute efficiency calibration is done using spontaneous parametric down-conversion (SPDC). SPDC is a nonlinear process where photons split in a crystal under the constraints of conservation of energy and momentum. In our experiment photons from an ultraviolet pump beam split into two lower energy down-converted photons. Because of the conservation of energy and momentum, the angle that the down-converted photons make with the pump beam is wavelength dependent. We collect 890 nm photons and their correlated 582 nm paired photons.

We send the collected 890 nm photons into one single photon detector and the 582 nm photons into another. If both detectors detect a photon at the same time (adjusted for differences in path length from the crystal to the detectors) we consider it to be a coincidence, or the detection of a correlated pair. Because photon pairs created from SPDC come from the same pump photon, the detection of one down-converted photon implies the existence of its correlated pair. The efficiency

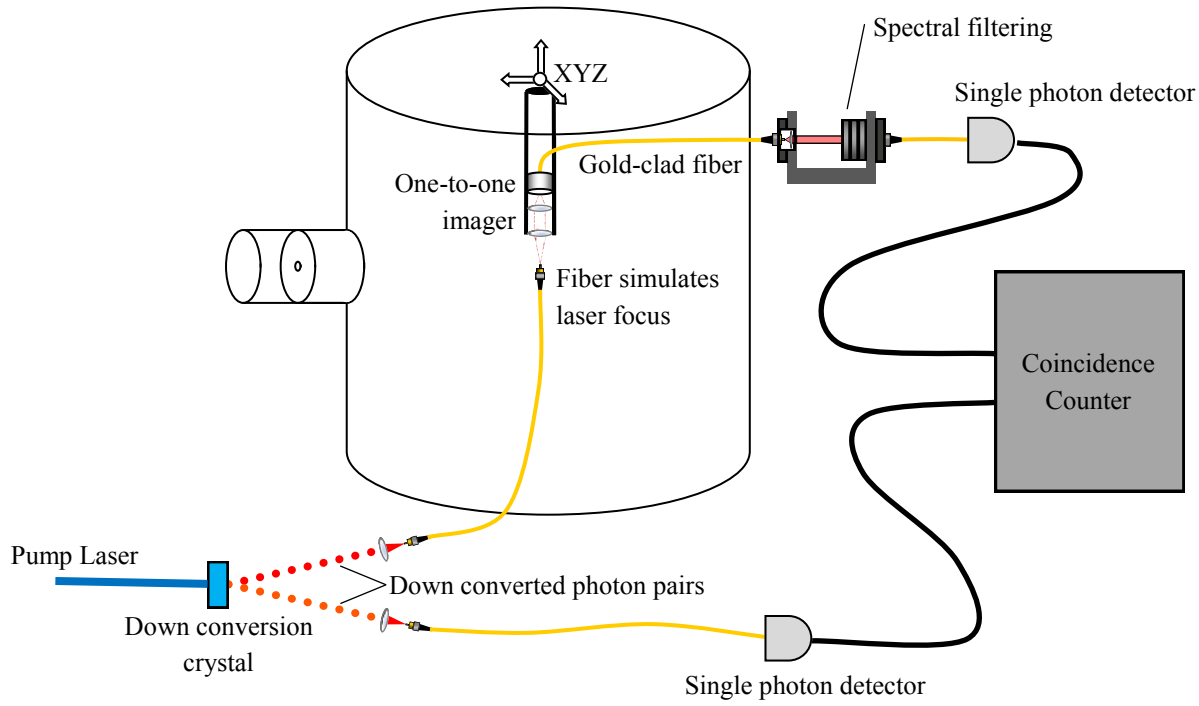

Figure 2.9 The setup for making the absolute measurement of collection efficiency. Light from a SPDC source is coupled into two single mode fiber optic cables. One cable couples directly into a detector. The other terminates in the interaction chamber, simulating a laser focus. The photons are collected by the one-to-one imager into another fiber optic cable which leads to the spectral filtering apparatus. It is then sent to a second detector. The two detectors are monitored for coincidence counts.

of a detection system at collecting and detecting correlated pairs is therefore the ratio of coincidences to total counts of one single photon detector. After measuring the efficiency of any arbitrary system, we add our optical collection system into the path of one channel of down-converted photons. The amount by which the coincidence rate decreases tells us the efficiency of the optical collection system.

To calibrate the optical collection system efficiency we first calculate the rate of coincidence counts while the beam paths for both the 890 nm and 582 nm photons couple directly into their respective detectors. This measurement is completely independent of the optical collection system. We then divert the down-converted 890 nm photons through the optical collection system without

changing before detecting them, as shown in Fig. 2.9. The down-converted photons are coupled into single-mode fibers. The 890 nm photons then exit the fiber where the intense laser focus would be in the interaction chamber. The photons then are coupled back into a fiber at the one-to-one imager and spectrally filter as described in sec. 2.6. After spectral filtering the photons are sent to the detector and we measure the new rate of coincidences. We again optimize the alignment using the coincidence count signal.

Because the optical collection system is not perfect not all of the photons exiting the fiber simulating the laser focus arrive at the detector. The ratio of the coincidence rate in this configuration compared to the coincidence rate without including the optical collection system gives us the efficiency of the optical collection system.

2.8 Intensity Measurement at the Focus

It is necessary to measure sufficient intensity at the laser focus to accelerate electrons to relativistic speeds. To measure the intensity, we use a time-of-flight spectrometer to measure the ionization states of atoms in the laser focus. By determining the highest ionization state achieved we can establish a lower bound for peak intensity at the focus. A diagram of time-of-flight spectrometer is given in Fig. 2.10. Atoms ionized in the laser focus are accelerated by a high positive voltage on the plate below the focus. The ions continue to accelerate until they pass through a copper wire mesh into a grounded drift tube. Their velocity is determined by their potential energy upon ionization, which is proportional to charge. The time delay t for the ions, then, is given by

$$t = d\sqrt{\frac{m}{2qV}}, \tag{2.1}$$

where d is the length of the drift tube, m is the mass of the ion, q is the charge of the ion, and V is the accelerating voltage.

The ions hit a micro-channel plate detector at the end of the drift tube. This plate is held at a

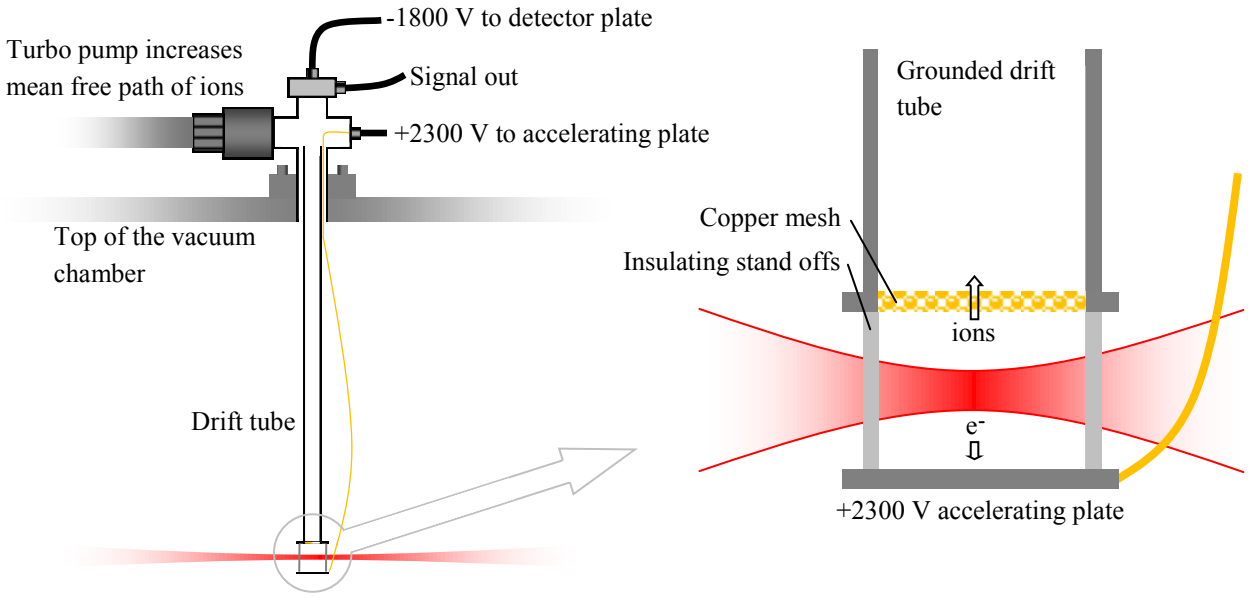

Figure 2.10 A cut away of the interaction chamber showing the time-of-flight spectrometer. Ions created in the laser focus are pushed up the drift tube by a positive accelerating voltage. They are detected after passing through the tube. A turbo pump helps to reduce collisions near the detector. The right image is a magnification of the laser and accelerating plate.

negative bias so that when the ions hit they eject cascades of electrons from the plate detector and create a voltage signal that can be measured by an external oscilloscope.

We use argon as the ion source to measure the intensity because the ionization intensities for its different ionization states range from 2.49×10^{14} W/cm^2 to 2.11×10^{18} W/cm^2. However, because argon has no charge states that ionize around 10^{17} W/cm^2, we also backfilled with neon. Neon will reach its seventh charge state at $1.50 \times 10^{1}7$ W/cm^2 [11]. Using both argon and neon gives us a good scale to measure intensities through our expected range. We follow the same procedure for ionizing argon as we do for helium: pump the chamber down to 10^{-8} torr and then backfill with the appropriate gas. This reduces noise due to water vapor and other contaminant gasses. Argon and neon's different ionization intensities along with the expected time delays for each ion are given in Table 2.1.

We are mainly interested in the most intense part of the laser focus. The other regions of the beam will not produce red-shifted signal. The volume that reaches adequate intensity to accelerate electrons relativistically is much smaller than the volume of the focus capable of ionizing the atoms. We need a small focal volume creating signal to efficiently image the signal as well as to avoid destructive interference between many electrons. We calculate the expected signal strength of each charge state for different peak intensities at the focus. This helps us anticipate what signal should be produced in out time-of-flight spectrometer at different intensities. The volume of a Gaussian beam reaching at least the intensity I is given by [10]

$$V = \pi \omega_0^2 z_0 [\frac{2}{9}(\frac{I_0}{I} - 1)^{3/2} + \frac{4}{3}(\frac{I_0}{I} - 1)^{1/2} - \frac{4}{3}\arctan(\frac{I_0}{I} - 1)^{1/2}]. \tag{2.2}$$

Here ω_0 is the beam waist, z_0 is the Rayleigh range, and I_0 is the peak intensity. At $I_0 = 5 \times 10^{18}$ W/cm^2 the signal from argon's ninth and tenth charge states should be very small because there are only about 50 atoms in the volume of the focus capable of producing each of these charge states at a pressure of one microtorr (close to the upper pressure limit for operating the time-of-flight spectrometer). This is a very small number of atoms compared with over 10^5 atoms in each

Ionization State of Argon	Time Delay (μs)	Ionization Intensity (W/cm^2)
1	7.10	2.49×10^{14}
2	5.02	5.80×10^{14}
3	4.10	1.22×10^{15}
4	3.55	3.20×10^{15}
5	3.18	5.06×10^{15}
6	2.90	7.62×10^{15}
7	2.68	1.93×10^{16}
8	2.51	2.61×10^{16}
9	2.37	1.57×10^{18}
10	2.25	2.25×10^{18}
Ionization State of Neon	Time Delay (μs)	Ionization Intensity (W/cm^2)
7	1.91	1.50×10^{17}
8	1.78	2.00×10^{17}

Table 2.1 The time delays (in our time-of-flight spectrometer) and ionization intensities corresponding to the ionization states for argon and neon.

of the first four charge states. The higher charge states arrive at the detector first, however, so the avoid being washed out by the strong signal from lower charge states. We average over many laser pulses to to able to see small detector responses at the time delays corresponding to these ions.

To maximize intensity we adjust the alignment of the grating pair and focusing mirrors while under vacuum using piezoelectric motors on the optical mounts. The alignments are adjusted while monitoring the oscilloscope readout to maximize signal from the highest ionization states. We find that adjustments in the grating separation affect the beam alignment slightly. The change in the beam path has to be corrected by manually adjusting the mirror focusing the light through the pinhole. This complicates the optimization of intensity at the focus.

Chapter 3

Results and Conclusions

In this chapter we report the results of the efficiency and intensity measurements. We also analyze the results and discuss directions for further work.

3.1 Collection System Efficiency

We make two measurements of the collection efficiency, a relative and an absolute calibration, as discussed in Sec. 2.7. The efficiency is important because it allows us to calculate total radiated power from measured power. While there is not a lower bound for an acceptable efficiency, lower efficiencies require us to take data for a longer period.

The relative method gives total collection system efficiency of 34.6%. This measurement is made as follows: Light from an 891.5 nm diode laser is coupled into a fiber optic cable. We then use a silicon optical power meter to measure the power at point (a), shown in Fig. 3.1. After optimizing the alignment of the signal collection apparatus we then measure power at points (b) and (c). Of total input power, as measured at point (a), 77.0% is transmitted to the spectral filtering apparatus. Only 44.9% of the the signal that makes it to the spectral filters arrives at the detector. This gives an overall efficiency of 34.6%. We find that the signal is attenuated more by the filtering

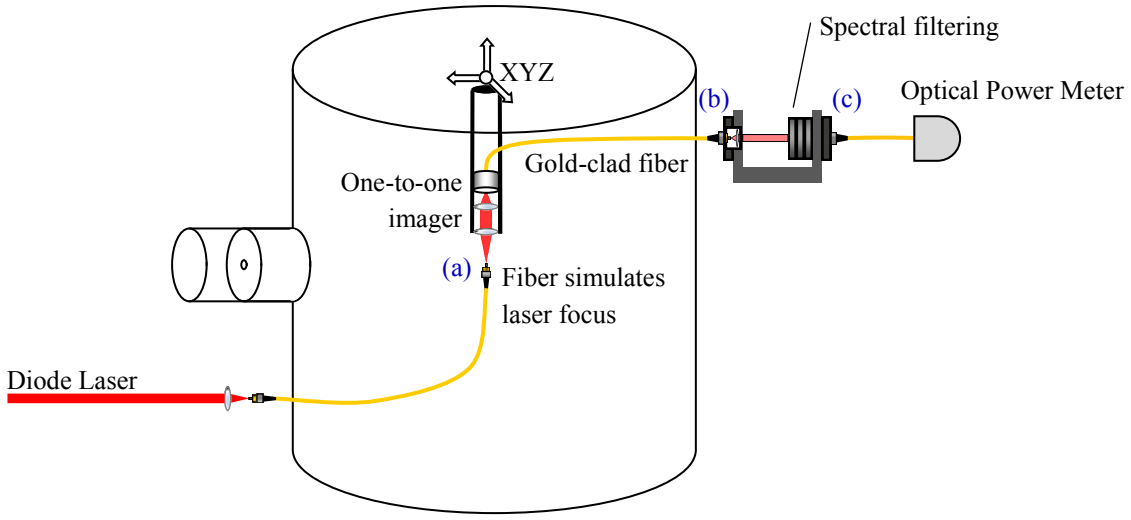

Figure 3.1 The relative efficiency measurement setup. Light from a diode laser is coupled into a fiber optic cable, which terminates in the interaction chamber at point (a) and simulates a laser focus. The power is measured at point (b) directly before the spectral filtering and at point (c) after the spectral filtering.

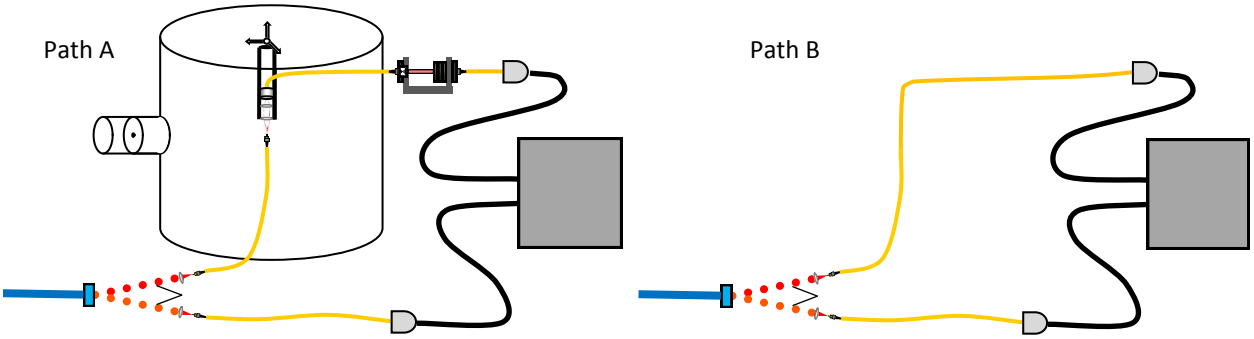

Figure 3.2 Absolute efficiency measurement layout, showing the paths corresponding to data given in Table 3.1. Path A includes the optical collection system. Path B is coupled directly from the crystal to the detectors.

process than by initial collection of light from the simulated focus.

The absolute measurement uses parametric down conversion and single photon detectors. We use a similar setup as for the relative measurement, shown in Fig. 3.2. We measure the average coincidence count rate passing through the signal collection apparatus. We also measure average

Path A Coincidences per two min	Path B coincidences per two min
393310	1757822
393198	1798234
373103	1797466
369083	1788996
392990	1777850
411450	1772822
407487	1744495
404475	1667335
402057	1704150
402138	1656285

Table 3.1 Coincidence data for two different paths: Path A goes through the collection apparatus, path B goes directly from the DC source to the detector.

count rate coupled directly from the down conversion source to the detector. The data from the absolute measurement is given in Table 3.1. The efficiency is the ratio of the coincidence rate for photons passing through the apparatus with the rate of the photons traveling directly to the detector. This gives an overall efficiency of 22.7%.

While the relative and absolute measurements of the collection efficiency differ by about 12%, they are consistent because the absolute measurement only places a lower bound on efficiency, which conceivably could be improved by better alignment of system components.

3.2 Intensity Measurement

We need to reach intensities on the order of 10^{18} W/cm^2 to produce an adequate red-shifted signal. We measure the intensity using the method outlined in sec. 2.8. The data measured using the time-

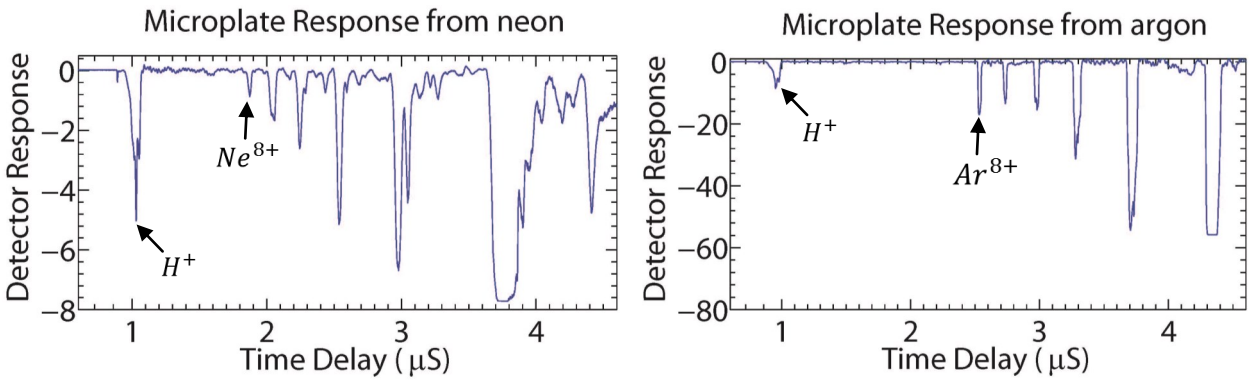

Figure 3.3 Oscilloscope data showing peaks corresponding to the arrival times for different neon on the left and argon on the right. The leftmost peak in each graph corresponds to hydrogen ions from impurities in the system.

of-flight spectrometer and oscilloscope are given is Fig. 3.3 and Fig. 3.4. We clearly measured the eighth ionization states of both argon and neon. The signal from the ninth charge state of argon is weak but appears noticeably above background when we take a selective average of data traces. We include all traces with signal greater than the noise threshold in the region between the peaks surrounding the expected position of the peak. This gives a lower bound on intensity of 1.57×10^{18} W/cm^2. The lower bound corresponds to the ninth charge state of argon, the ion requiring the highest intensity that is created in our focus. We did not establish an upper bound on the intensity because the mass to charge ratio of the tenth charge state of argon is degenerate. Comparing the size of the ninth peak of argon to the degenerate ion signal we cannot distinguish between signal from the two species of ion.

3.3 Analysis

The collection system efficiency is acceptable for the requirements of the experiment. The percentage of signal reaching the detector is high enough to observe the strength of single electron radiation from an intense laser focus. The main parameter of interest in the overall experiment is

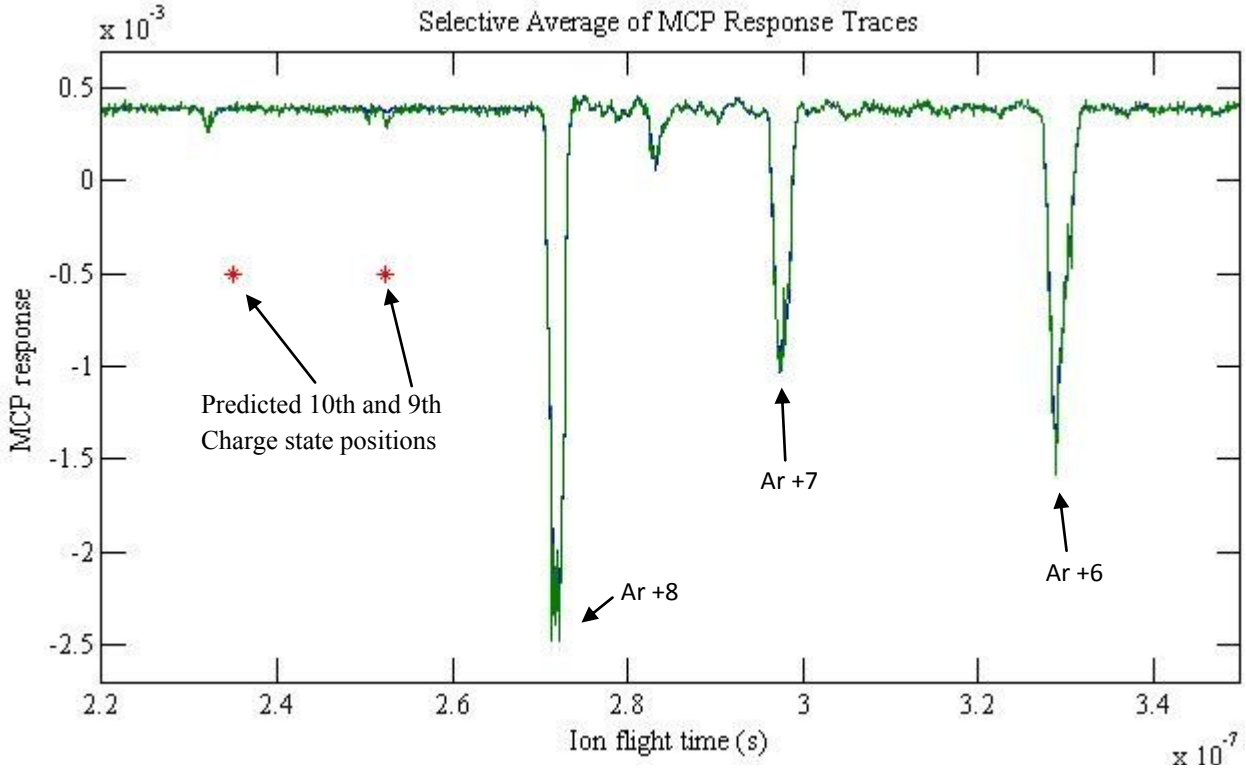

Figure 3.4 Oscilloscope data showing the ninth charge state of argon next to the eighth, seventh, and sixth charge states of argon (left to right). The data shown is a selective average of 458 traces out of 2000 total traces.

total radiated signal of the electrons in an intense laser focus of known intensity. Using our measured values for collection efficiency we can calculate the total radiated signal from our collected signal.

Our measured intensity is sufficient to produce the red shifted signal we seek. It the uncertainty in the actual achieved intensity is large because the tenth charge state of argon has a degenerate mass to charge ratio with a contaminant gas. If greater accuracy is required to conclusively match predicted radiation to theory it may be necessary to use a different ion, such as krypton, to make the intensity measurement.

3.4 Directions for Further Work

The next step is characterizing the background noise. We need to understand the background noise and discriminate against it well enough to be confident that we can measure the scattered signal over the background.

There is some shot-to-shot variation in the energy (and thus intensity) of our laser pulses. This needs to be characterized so that we know if lower energy pulses are still capable of producing red-shifted signal photons. If they are not, we need to be able to account for the average number of pulses with insufficient intensity in our calculation of the electrons' total radiated signal.

Once these challenges are overcome we will be ready to make final measurements of radiation scattered by single electrons. This will help us shed light onto the nature of an electron's charge distribution.

Bibliography

[1] P. Rodgers, "The double-slit experiment," http://physicsworld.com/cws/article/print/2002/sep/01/the-double-slit-experiment (Accessed January 23, 2013).

[2] J. Peatross, C. Müller, and C. H. Keitel, "Electron wave-packet dynamics in a relativistic electromagnetic field: 3-D analytical approximation," Opt. Express **15,** 6053–6061 (2007).

[3] E. A. Chowdhury, I. Ghebregziabiher, and B. C. Walker, "Larmor radiation from the ultra-intense field ionization of atoms," J. Phys. B **38,** 517–524 (2005).

[4] J. Peatross, C. Müller, K. Hatsagortsyan, and C. Keitel, "Photoemission of a Single-Electron Wave Packet in a Strong Laser Field," Phys. Rev. Lett. **100,** 153601 (2008).

[5] J. P. Corson, J. Peatross, C. Müller, and K. Z. Hatsagortsyan, "Scattering of intense laser radiation by a single-electron wave packet," Phys. Rev. A **84,** 053831 (2011).

[6] P. Krekora, "Retardation and Kinematic Relativistic Effects in Scattered Light," Laser Phys. **12,** 455–462 (2002).

[7] J. Roman, L. Roso, and H. Reiss, "Evolution of a relativistic wavepacket describing a free electron in a very intense laser field," J. Phys. B **33,** 1869–1880 (2000).

[8] J. Roman, L. Playa, and L. Roso, "Relativistic quantum dynamics of a localized Dirac electron driven by an intense-laser-field pulse," Phys. Rev. A. **64,** 063402 (2001).

[9] J. P. Corson and J. Peatross, "Quantum-electrodynamic treatment of photoemission by a single-electron wave packet," Phys. Rev. A **84,** 053832 (2011).

[10] E. Cunningham, "Photoemission by Large Electron Wave Packets Emitted out the Side of a Relativistic Laser Focus," Master thesis (BYU, Provo, UT, 2011).

[11] S. Bergeson and J. Peatross, "571 Lecture 38: Strong-Field Ionization," http://www.physics.byu.edu/faculty/bergeson/physics571/old/lecturenotes/Physics571L38.pdf (Accessed February 19, 2013).

Index